

Conductance interference in a superconducting Coulomb blockaded Majorana ring

Ching-Kai Chiu,¹ Jay D. Sau,¹ and S. Das Sarma¹

¹ *Condensed Matter Theory Center and Joint Quantum Institute and Station Q Maryland,
Department of Physics, University of Maryland, College Park, MD 20742, USA*

(ΩDated: March 10, 2022)

By tuning the magnetic flux, the two ends of a 1D topological superconductor weakly coupled to a normal metal as a ring-shaped junction can host split Majorana zero modes (MZMs). When this ring geometry becomes Coulomb blockaded, and the two leads come into contact with the two wire ends, the current moves through the superconductor or the normal metal as an interferometer. The two-terminal interference conductance can be experimentally measured as a function of gate voltage and magnetic flux through the ring. However, a 4π periodicity in the conductance-phase relation (often considered the hallmark of MZMs), which can arise both in a topological superconductor and in a trivial metal, cannot establish the existence of MZMs. We show that the trivial metal phase can be ruled out in favor of a topological superconductor by studying persistent conductance distribution patterns. In particular, in the presence of MZMs, the conductance peak spacings of the Coulomb blockaded junction would manifest line crossings as the magnetic flux varies. The locations of the line crossings can distinguish line crossings stemming from the trivial metal.

Pursuing fault-tolerant quantum computation has been a primary motivation in searching for robust non-Abelian topological excitation in nature. A localized Majorana zero mode (MZM), perhaps the most promising candidate, has been actively studied theoretically¹⁻⁴ and experimentally⁵⁻¹¹. Although Majorana braiding schemes for quantum computing have been proposed in the literature¹²⁻¹⁴, it is unclear at this stage whether sufficient experimental evidence exists providing compelling support for the existence of MZMs. In this work, we propose an interference experiment in a Coulomb blockaded topological superconductor ring with magnetic flux in order to provide sufficient and definitive evidence for the existence of MZMs in semiconductor nanowires. It turns out that the theoretical analysis of MZM conductance in a ring structure is quite subtle.

A Coulomb blockade device is small enough so that inserting electrons into the device costs a significant amount of Coulomb charging energy, which dramatically affects the experimental behavior including MZM physics. Coulomb blockade physics has been incorporated in the theoretical study of topological superconductors in the context of tunneling transport experiments¹⁵⁻¹⁹. An important experimental breakthrough in Coulomb blockaded nanowires is the two-terminal conductance measurement in a spin-orbit coupled superconducting semiconductor nanowire under an applied magnetic field¹¹. The observed oscillations of the conductance peak spacings¹¹ bring new physics to measure MZMs. The superconducting Coulomb blockaded nanowire manifests both $1e$ and $2e$ tunneling signatures through the system with the $2e$ effect presumed to be the ordinary Andreev transport. As the lowest energy level of the wire is less than the Coulomb blockade charging energy E_c , the $1e$ tunneling dominates transport and exhibits $1e$ periodicity as a function of the gate voltage V_g . In this manuscript, we focus on the $1e$ tunneling region to study the MZM signatures since this appears to be the prominent transport channel in the Coulomb blockade

device.

Coherent electron *teleportation*^{17,20}, which is the MZM smoking gun signature, has been discussed in the theoretical literature. In this scenario, an electron that is coherently transported from one Andreev Bound state^{16,21} can be observed by detecting 4π periodic Aharonov-Bohm (A-B) oscillations, as electrons travel in a ring-like geometry similar to the one shown in Fig. 1.

Here we consider the possibility of the A-B oscillations that would arise because of teleportation. For this purpose, we consider the setup in Fig. 1, where an electron transported between the leads L and R can either be teleported through the Majorana wire (shown in blue) or through the normal segment, leading to current interference if the system is phase coherent (i.e. very low temperature). The entire system is Coulomb blockaded to support a definite number of electrons. When the blue region in Fig. 1 is an ideal spin-orbit coupled nanowire, the application of a Zeeman field (above a critical field¹⁻³) should transform the wire into the topological phase with MZMs localized at the wire ends. The transported electrons in the topological phase would have two paths to go from L to R – one through the wire and the other through the red quantum dot. The interference of the electrons between these distinct paths is expected to manifest itself in an h/e flux dependence of the conductance of the system^{15,17,22,23}. These oscillations of 4π -periodicity can also be thought of as arising from the fractional Josephson effect^{22,24-27} in the ring Josephson junction shown in Fig. 1. The Coulomb blockade constrains the number of particles in the system and in some situations may lead to 4π -periodicity of superconducting transport properties of the system²⁸.

Specifically, in this paper, we consider a microscopic model for normal transport in the system shown in Fig. 1. An important question here is how to distinguish the 4π -periodic MZM oscillations from the trivial A-B oscillations in a normal metal ring. The problem, of course, is that one cannot a priori rule out the

possibility of non-superconducting A-B transport in this ring geometry leading to A-B oscillations, which are always 4π -periodic. Despite the fact that the 4π -periodic oscillation (i.e., the fractional Josephson effect) strongly distinguishes topological superconductors from conventional superconductors (the regular Josephson effect), 4π also happens to be the periodicity of A-B oscillations where a non-superconducting metal ring replaces the blue region in Fig. 1. A small gap or near critical superconductor has long correlation lengths similar to a normal metal and can also manifest 4π -periodic oscillations. Hence, the observation of the fractional Josephson effect^{6,29–31} is not conclusive evidence of MZM existence unless normal A-B effect can be decisively ruled out. Solutions proposed to this problem, such as varying the charging energy¹⁶, do not appear to be feasible in the present experimental setups¹¹. This motivates us to compare the conductance spectra of such gapless trivial states to the topological system. Interestingly, we find that the conductance of the critical/gapless system indeed manifests 4π -periodic oscillations similar to the topological system. Therefore, 4π -periodic oscillations cannot be the sole means of identifying topological phases. However, a measurement of the excitation gap by comparing the conductance peak spacings, which is a feasible measurement already used in [11], allows one to distinguish the topological phase from the critical/gapless trivial system.

The remainder of this paper is organized as follows. In sec. I, we first establish an interferometer setup for topological superconducting nanowire as well as trivial metal one as a comparison. To propose the observable features of the topological superconductivity and to avoid quasiparticle poisoning, we consider the interferometer is small enough to become Coulomb blocked and further review the recipe to compute the conductance of the superconducting Coulomb blockade. In sec. II, we show the conductance as a function of the magnetic flux for the different interferometers and compare the conductance features of the topological superconductivity with the trivial superconductor and the trivial metal. Sec. III is devoted to the study of the conductance peak spacings, which are another observable revealing the topological superconductivity. In sec. 6, we show the appearance of the MZMs can be manipulated by adjusting the Zeeman field along the spin orbital coupling in the wire. Finally, in Sec. V we conclude the paper and give an outlook on future research.

I. INTERFEROMETER SETUPS

The experimental setup we propose is shown schematically in Fig. 1 with current leads L and R in contact with the ends of a superconducting proximitized nanowire in the presence of spin-orbit coupling. By tuning Zeeman splitting strength, the nanowire passes through the topo-

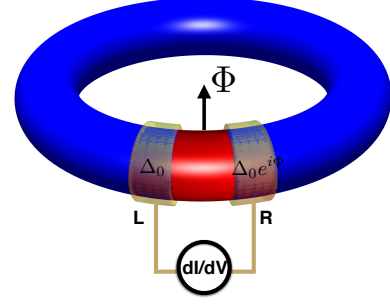


FIG. 1. The schematic of the Coulomb blocked Majorana ring. The blue region represents the superconducting nanowire ($1 \leq j \leq L$), while the red color ($j = 0$) represents a non-superconducting site weakly coupling with the two wire ends. The two leads (dark yellow) come into contact with the wires ends ($j = 1, L$) to measure the conductance as the gate voltage V_g applied on this ring and the magnetic flux Φ goes the middle of the ring. The current moves from one lead to the other through the superconductor or the non-superconducting site as an interferometer.

logical quantum phase transition (TQPT), then hosting MZMs at the wire ends. In this topological superconductivity region, we further destroy the MZMs by introducing the coupling between the two wire ends and a non-superconducting metal to form a ring geometry as illustrated in Fig. 1, and further insert magnetic flux Φ in the unit of flux quantum $h/2e$ going through the middle of the ring. The the ring setup is small enough to become Coulomb blocked. In this manuscript, we numerically compute the two-terminal conductance of the Coulomb blocked ring and propose *observable* and *distinguishable* MZM features. In particular, we show that the evidence for the topological superconductor hosting MZMs is the line crossings of the conductance peak spacings at the specific values of the superconducting phase differences between the nanowire ends stemming from the inserting magnetic flux.

We start with the model of the 1D superconducting proximitized semiconductor nanowire with spin-orbit coupling in the presence of a field-induced Zeeman spin splitting^{2,3}. As its two ends weakly couple with a non-superconducting site, the lattice Hamiltonian can be written as

$$\begin{aligned} \hat{H}_{\text{BdG}}^{\text{ring}} = & \sum_{1 \leq j \leq L} \left\{ C_j^\dagger \left[(2t - \mu)\tau_z\sigma_0 + \Delta_0\tau_y\sigma_y + V_z\tau_z\sigma_z + V_y\tau_0\sigma_y \right] C_j \right. \\ & + \left. \left[C_{j+1}^\dagger (-t\tau_z\sigma_0 + \alpha i\tau_z\sigma_y) C_j + h.c. \right] \right\} \\ & + w \left(C_0^\dagger\tau_z C_1 + C_0^\dagger\tau_z C_L + h.c. \right), \end{aligned} \quad (1)$$

where Pauli matrix σ_α represents spin degree of freedom and $C_j = (c_{\uparrow j}, c_{\downarrow j}, c_{\uparrow j}^\dagger, c_{\downarrow j}^\dagger)^T$ indicates the vector including the Fermion annihilation and creation operators represented by τ_α . The last term in the Hamilto-

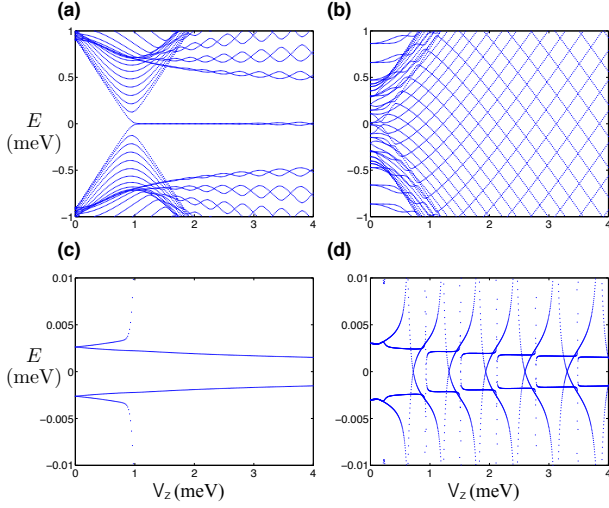


FIG. 2. Energy spectra for the single nanowire and the interferometer ring as illustrated in Fig. 1. In the absence of the non-superconducting site (a,b) represents the energy spectra of the semiconductor nanowire with superconductivity $\Delta_0 = 0.9\text{meV}$ and without superconducting gap $\Delta_0 \rightarrow 0$ meV respectively. (c,d) show in the absence of the magnetic flux ($\Phi = 0$) the energy spectra of the superconducting and trivial metal rings with the coupling ($w = 0.1\text{meV}$) between the non-superconducting site ($j = 0$) and the superconducting nanowire ends ($j = 1, L$). This coupling in the superconducting ring always keeps the lowest energy level away from zero, although there is a low-energy state in the non-superconducting site as a normal metal. On the other hand, in non-superconducting ring, as V_z increases, the energy level sometimes reaches to zero energy. The values of the remaining parameters are based on [19] with the lattice constant $a = 15\text{nm}$: hopping strength $t = 6\text{meV}$ (effective mass $= 1.5 \times 10^4 \text{eV}/c^2$), spin-orbit coupling $\alpha = 1.2\text{meV}$, superconducting order parameter $\Delta_0 = 0.9\text{meV}$, the chemical potential $\mu = 0.2\text{meV}$, and the length of the wire $L = 80$ ($1.2\mu\text{m}$). These parameters are used for the following conductance calculation.

nian represents a non-superconducting state (C_0) weakly coupling with the two ends of the superconducting wire. (We note that this non-superconducting normal arm is about the same length as the superconducting wire. We specially consider large Fermi velocity so that the normal arm is effective short.) The left and right leads come into contact with the first site C_1 and the last site C_L for the measurement of the two-terminal conductance as illustrated in Fig. 1. The results of the observables closely depend on the value of the Zeeman field (V_y) in parallel with the direction of the nanowire spin orbital coupling. To simplify the problem, we consider only the Zeeman field (V_z) perpendicular to the direction of the spin orbital coupling first and recover non-zero V_y later.

The magnetic flux Φ through the middle of the ring can be addressed by the Peierls substitution in the BdG

Hamiltonian (1): for $j \neq 0$

$$C_j^\dagger \Delta_0 \tau_y \sigma_y C_j \rightarrow C_j^\dagger \Delta_0 [\cos(2j\phi) \tau_y \sigma_y + \sin(2j\phi) \tau_x \sigma_y] C_j, \quad (2)$$

$$C_{j+1}^\dagger (-t\tau_z \sigma_0 + \alpha i \tau_z \sigma_y) C_j \rightarrow C_{j+1}^\dagger [(\tau_z + \tau_0)e^{-i\phi} + (\tau_z - \tau_0)e^{i\phi}] \frac{-t\sigma_0 + \alpha i \sigma_y}{2} C_j, \quad (3)$$

where $\phi = \Phi/2L$. The superconducting phase difference between the two wire ends is given by $\Phi(L-1)/L \sim \Phi$ in large- L limit. By performing the exact diagonalization for $\hat{H}_{\text{BdG}}^{\text{ring}}$ of the superconducting nanowire without non-superconducting site (C_0), the calculated energy spectrum in Fig. 2(a) shows that the TQPT is located at $V_{zc} = \sqrt{\Delta_0^2 + \mu^2} = 0.922\text{meV}$. Furthermore, in the presence of the non-superconducting site (C_0) and the coupling $w = 0.1\text{meV}$, the energy level always has a small gap as the Zeeman field (V_z) increases as shown in Fig. 2(c). We label E_p in ascending order as the quasi-particle energy levels of the ring with respect to the BCS ground state and E_1 represents the energy difference between the lowest energy BCS states with the odd and even parities. (At $\Phi = 0$, $V_z = 0$, we choose $E_1 > 0$ for the BCS ground state with even parity.) The Zeeman field V_z and the magnetic flux Φ vary, the BCS wavefunction adiabatically evolves with its fermion parity remaining fixed. To compare features of the topological superconductivity, we introduce the trivial metal nanowire with superconducting gap $\Delta_0 \rightarrow 0$ as the trivial topological phase. The spectra of the metal nanowire and ring exhibits multiple zero energy crossings as shown in Fig. 2(b,d).

Now we consider a situation where the ring becomes Coulomb blockaded with charging energy E_c . To compute the conductance, we use the already developed master equation formalism¹⁹ by assuming that the tunneling rates between the leads and the wire ends are much less than the system temperature (T) and the energy level spacing. We use the tunneling rates between the leads and the wire ends defined in [19]. Furthermore, we assume that the charging energy E_c ($= 2\text{meV}$ in the following calculation) is large enough so that only the two lowest energy levels $U(N+1)$ and $U(N)$ of the electrostatic energy

$$U(N) = E_c(N - n_g)^2, \quad (4)$$

are involved in transport with the energy levels of the other electron numbers being too high to be important. The gate voltage (V_g) of the ring is an experimentally controllable physical parameter, which is proportional to n_g since $n_g = CV_g/e$, where C is the ring capacitance. In the following, the conductance is computed as a function of normalized gate voltage (n_g) and the flux Φ . In a superconductor, since the physics is not altered by the transformation $N \rightarrow N+2$ and $n_g \rightarrow n_g+2$ in Eq. (4) (adding a Cooper pair), the conductance as a function of n_g exhibits $2e$ periodicity. We further assume that for

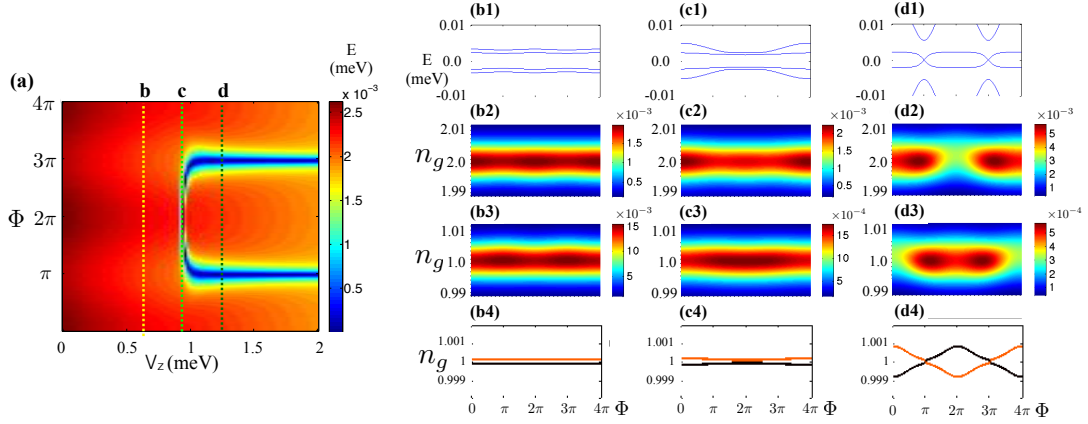


FIG. 3. For the superconducting interferometer, quasiparticle and quasihole spectrum, conductance, and conductance peak spacings as the Zeeman potential V_z , which is perpendicular to the spin-orbital direction, is tuned to change the phase from the conventional phase (panels b) ($V_z = 0.75\text{meV}$), through the TQPT (panels c) ($V_z = 0.922\text{meV}$) to the topological phase (panels d) ($V_z = 1.2\text{meV}$). Panel (a) shows the positive energy level closest to zero energy and the blue color indicates the presence of the MZMs localized at the ends of the superconducting nanowire at $\Phi = \pi, 3\pi$. The two blue color lines merge at the TQPT ($V_z = 0.922\text{meV}$). Panels (1) represent the energy spectra of the ring at fixed V_z 's, while panels (2,3) show the conductance at temperature $T = 0.01\text{meV}$ with even and odd particle number N respectively. As expected all quantities in panels (b1,b2,b3) are 2π periodic in the flux Φ . In contrast, in the topological phase due to the line crossings ($E_1 = 0$) at $\Phi = \pi, 3\pi$ (panel d1)^{25,32}, the conductance oscillations (panels d2,d3), which are 4π periodic, are distinguishable from the conventional superconductor case. While the spectra are 4π periodic in the critical region (panel c1), which is similar to a conventional metal, the conductance oscillations (panels c2,c3) are 4π periodic. Panels (4) represent the conductance peak spacings for even S_e (black) and odd S_o (orange) parities at $T = 0.01\text{meV}$. The important MZM feature is that the crossing of the two parity lines are *fixed* at $\Phi = \pi, 3\pi$ as V_z varies in the topological region since panel a shows MZMs are always located at $\Phi = \pi, 3\pi$; elsewhere, the lines of the spacings are flat and close to 1.

the trivial metal ring also has this $2e$ -periodicity since the ring is deposited on the top of the superconductor. Hence, computing the conductance with even and odd particle number (N) is enough to describe the interference phenomenon.

We have to define the lowest energy BCS states with N and $N + 1$ particle numbers respectively as base states, since the Coulomb blockade conductance computed in the master equation formalism [19] mainly based on these base states. At the beginning ($V_z = 0, \Phi = 0$), all of the quasiparticle energy levels E_i are chosen to be positive and the lowest energy BCS state with even particle number is defined to obey

$$a_{E_p}|\text{BCS}_e\rangle = 0, \quad (5)$$

for all p , where a_{E_p} is the quasiparticle annihilation operator. Hence, $|\text{BCS}_e\rangle$ is the BCS ground state. As V_z and Φ vary, the fermion *parity* of the base state should be fixed and the lowest positive energy level E_1 might reach zero as a band crossing. After this energy band crossing, $|\text{BCS}_e\rangle$ evolves to the BCS first excited state still obeying (5) and the value of the energy level E_1 is changed to negative from positive. Although the entire quasiparticle and quasihole energy spectra ($\pm E_i$) are identical, as the base state with even fermion parity has negative E_1 , the different quasiparticle energy spectra ($-|E_1|, E_{i \neq 1}$) and ($|E_1|, E_{i \neq 1}$) do lead to the two distinguishable conductances. As V_z and Φ continuously change, after the

next zero energy crossing, the base state with the fixed fermion parity evolves back to the BCS ground state until the third band crossing and so on.

Similarly, at the beginning ($V_z = 0, \Phi = 0$), the lowest energy BCS state with odd particle number obeys

$$a_{-E_1}|\text{BCS}_o\rangle = 0, \quad a_{E_{p \neq 1}}|\text{BCS}_o\rangle = 0, \quad (6)$$

where the quasiparticle annihilation operator a_{-E} with energy $-E$ is equivalent to the quasihole annihilation operator a_E^\dagger with energy E . After the first gap closes $E_1 = 0$, with the fixed parity $|\text{BCS}_o\rangle$ becomes the BCS ground state from the BCS first excited state. When the second gap closing is passed, $|\text{BCS}_o\rangle$ goes back to the BCS first excited state. We carry out our numerical calculations following the parity-fixed prescription above.

II. COULOMB BLOCKADED CONDUCTANCE

The conductance and the conductance peak spacings can reveal some features of the topological superconducting ring in the trivial ($V_z < V_{zc}$, Fig. 3(b)), TQTP ($V_z = V_{zc}$, Fig. 3(c)), and topological ($V_z > V_{zc}$, Fig. 3(d)) regions. The MZMs with zero energy appear at $\Phi = 0, 3\pi$ after TQTP as illustrated in Fig. 3(a), which shows the lowest energy level of the superconducting ring as V_z and Φ vary. In the gapped superconductor ($V_z \neq V_{zc}$)

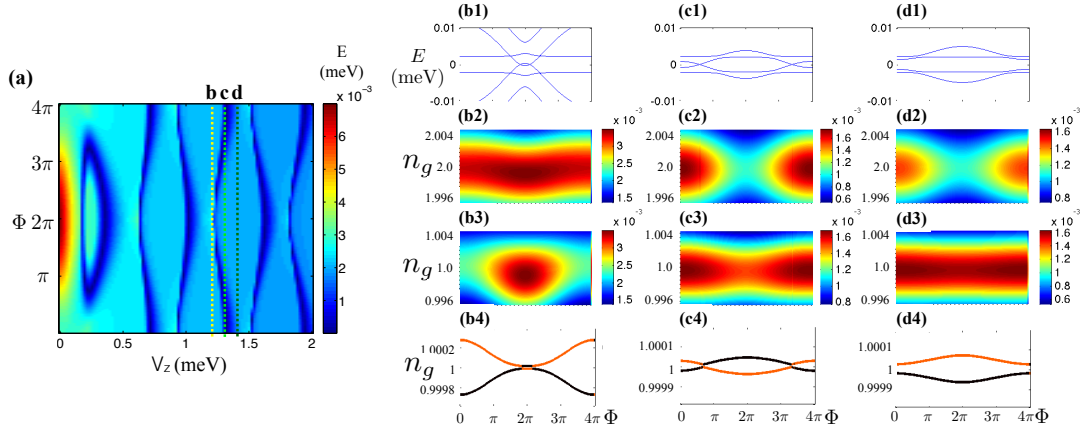


FIG. 4. For the trivial metal interferometer, quasiparticle and quasihole spectrum, conductance, and conductance peak spacings show the features of A-B effect. Panel (a) shows the positive energy level closest to zero energy and the blue color indicates zero energy modes, which are not MZMs. A-B effect exhibits 4π -periodicity of Φ in the trivial metal interferometer ring $\Delta_0 \rightarrow 0$ for different fixed values of V_z : (b) 1.225 meV (c) 1.3 meV (d) 1.375 meV. Panels (1,2,3,4) represent the identical physical quantities in Fig. 3 respectively. Panels (1) show the Φ -locations of the zero energy modes move around as V_z vary and even the zero energy modes vanish at some V_z 's. The zero energy modes can be reflected by the crossing of the conductance peak spacings in panels (4).

the quasiparticle and quasihole energy spectrum ($\pm E_i$) (Fig.3(b1,d1)) always exhibits the 2π -periodicity of the magnetic flux. As the flux increases from 0 to 2π , in the absence of the gap closing (Fig.3(b1)), the quasiparticle energy levels E_p evolve back to the original spectrum. Hence, since the spectra with $\Phi = 0, 2\pi$ are identical, the conductance always has 2π -periodic oscillation. The coupling between the normal site and the wire ends completely keeps the entire system gapped ($E_1 \neq 0$) in the trivial region ($V_z < V_{zc}$) as shown in the ring spectrum of Fig. 3(a,b1); thus, the conductance oscillation is 2π -periodic and consistent with the numerical result in Fig. 3(b2,b3).

Near the TQTP point, the energy spectrum (Fig. 3(c1)) exhibits the periodicity of 4π . Hence, the conductance oscillations in Fig. 3(c2,c3) also are 4π -periodic. This 4π periodicity is similar with the conductance of the trivial metal ring, which will be discussed later.

In the topological region ($V_z > V_{zc}$), as the flux is adjusted to $\pi, 3\pi$, MZMs appear on the ends (the first and L -th sites) of the nanowire³² so that the energy gap is closing ($E_1 = 0$) as shown in Fig. 3(c1). The lowest quasiparticle energy level E_1 is changed to be negative from positive at $\Phi = \pi$ and back to positive as Φ passes through 3π . Since the energy level E_1 goes back to the original value after 4π flux, the system with $\Phi = 0, 4\pi$ is identical. Thus, beyond the TQPT point, the 4π -periodic quasiparticle energy spectrum produces 4π -periodic oscillation as shown in in Fig. 3(c2,c3).

To distinguish topological superconductivity from normal-metal A-B effect, we turn off the superconductivity $\Delta_0 \rightarrow 0$ in the nanowire and the lowest energy spectrum of the normal metal ring as a function of V_z

and Φ is shown in Fig. 4(a). Due to the nature of the normal metal, the zero energy modes, which are definitely not MZMs, appear several times. The spectrum exhibits the 4π periodicity of Φ , which can be seen the spectra, as Φ varies, at the three fixed V_z values in Fig. 4. It is expected that the conductances of the Coulomb blockaded normal metal ring have the 4π periodicity of Φ in Fig. 4(2-3). The normal metal conductance shows the non-superconducting wire has the similar 4π -periodicity patterns with the topological superconductor ($V_z \geq V_{zc}$) in Fig. 3(c2,c3,d2,d3).

The observation of 4π periodicity cannot directly lead to the conclusion of the MZM existence, since in the presence of the normal metal the conductance oscillation is also trivially 4π -periodic as the manifestation of the usual A-B effect¹⁶. (This superficial agreement between interference phenomena in a topological superconducting ring and a normal metal ring arises simply from both systems manifesting $1e$ coherent transport for different reasons.) Although the conductance-phase relation has the same 4π periodicity in both cases, the conductance distributions as a function of Φ and n_g are distinguishable. Since in the topological region the lowest energy level (Fig. 3(a)) does not significantly change as V_z varies, the conductance distribution patterns (Fig. 3(d2,d3)) *persists* at any V_z in the entire topological region whereas the patterns alter *dramatically* as V_z varies in the normal metal; these features are confirmed in our numerical simulation. The observation of the conductance distribution persistence in the topological region is the key feature distinguishing the topological superconductor and the normal metal.

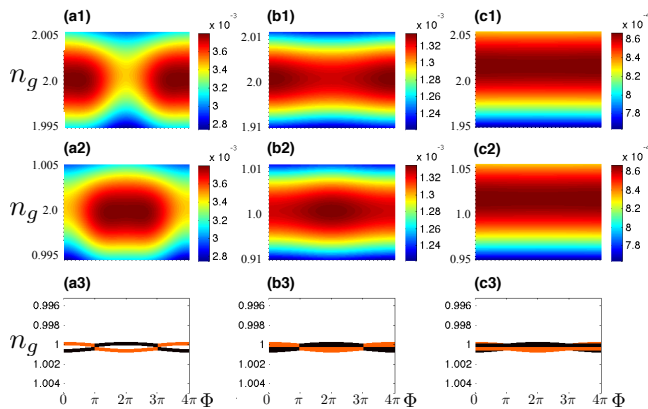


FIG. 5. The conductance and the conductance peak spacing in the topological region $V_z = 1.2\text{meV}$ (Fig. 3(c1)) at different temperatures (a) $T = 0.02\text{meV}$ (b) $T = 0.07\text{meV}$ (c) $T = 0.3\text{meV}$. Panels (1,2,3) represent the identical physical quantities in Fig. 3(2,3,4) respectively, except for temperature. High temperature broadens the conductance peak and suppresses the oscillation of the conductance peak spacings.

III. CONDUCTANCE PEAK SPACINGS

The measurement of the conductance peak spacings is an important observable to probe the presence of the MZMs possessing zero energy. The reason to study the conductance peak spacings is that the spacings were successfully measured in the Coulomb blocked superconducting wire¹¹. The location of the conductance peaks are determined by the maximum conductance values of n_g at fixed flux Φ and V_z . At low temperature ($T \ll E_2$), their gate voltage locations for even and odd N are given by $n_g^e(N) = N - E_1/2E_c$ and $n_g^o(N) = N + E_1/2E_c$ respectively, where the resonant $1e$ tunneling occurs. The important quantities studied in the Coulomb blockade experiment¹¹ are the even and odd peak spacings

$$S_o = n_g^e(N+1) - n_g^o(N) = 1 - E_1/E_c, \quad (7)$$

$$S_e = n_g^o(N+1) - n_g^e(N) = 1 + E_1/E_c, \quad (8)$$

which are the differences between the two closest conductance peaks. The spacings directly depict the lowest energy spectrum. However, when $E_2 \lesssim T$ the 2nd energy level affects the location of the conductance peak, Eqs. 7,8 do not hold. This is the reason we use the master equation formalism for a superconducting Coulomb blockade to compute conductance in the high-temperature generic situations since the low-temperature constraint is unlikely to be satisfied experimentally¹⁹. However, even at higher temperature, when $E_1 = 0$ in the presence of the MZMs, the even and odd peak spacings¹⁹ are identical due to the $1e$ tunneling resonance. Hence, the energy level crossings at zero energy in the superconducting spectrum are directly reflected by the crossing of the conductance peak spacings.

We first discuss the conductance peak spacings for the

superconducting ring as shown in Figs. 3(4). In the topological region, the appearance of the MZMs with $E_1 = 0$ at $\Phi = \pi, 3\pi$ leads to the crossing of the two conductance peak spacing lines. It is confirmed by our numerical simulation that this crossing feature can be seen at any V_z value in the topological region. Although, as shown in Fig. 3(d1) near $\Phi = \pi, 3\pi$, Eqs. 7,8 do not hold due to the second energy level, which is smaller than the temperature ($E_2 < T = 0.01\text{meV}$), 4π -periodicity of the conductance peak spacing (Fig. 3(d4)) shares clear similarity with the lowest energy spectrum (Fig. 3(d1)). On the contrary, in the trivial region and the TQPT, the flatness of the lowest energy level and the suppression of the second lowest energy level ($< T = 0.01\text{meV}$) lead to flat conductance peak spacing lines without the crossing as shown in Fig. 3(b4,c4), contrasting with the topological situation. Therefore, in going from the trivial system to the topological superconductor, the transition of the conductance peak spacing from flat lines to 4π -periodic oscillation and line crossings should be observed.

The normal metal ring also exhibits line crossings in the conductance peak spacings. However, as shown in Figs. 4(4), the crossings move to different values of Φ and even vanish as the Zeeman splitting V_z varies. Since the crossings are not fixed for the trivial metal ring as V_z varies, the fixed line crossings of the conductance peak spacings (at $\Phi = \pi, 3\pi$ only for $V_y = 0$) can be the evidence for MZMs.

Ideally, the temperature is expected to be low so that the conductance peak spacings can faithfully depict the lowest energy spectrum. High temperature might alter the observable and disguise the MZM evidence. Fig. 5(1,2) shows that in the topological region, the conductance peak is broadened at higher temperature and the difference between the two conductance peak spacings are suppressed by higher temperature. As the temperature is too high, 4π periodicity of the conductance-phase relation cannot even be observed as shown in Fig. 5(1,2) and the conductance peak spacing becomes flat as the temperature increases as shown in Fig. 5(3).

IV. ZEEMAN FIELD ALONG THE SPIN ORBITAL COUPLING DIRECTION

For this superconducting semiconductor nanowire interferometer, MZMs with exact zero energy appear at $\Phi = \pi, 3\pi$ due to an effective time reversal symmetry. However, in reality this symmetry can be easily broken by applying magnetic field (V_y) along the spin-orbital coupling direction. In this section, we derive the flux location of the MZMs as a function of the Zeeman field along the spin-orbital direction. Our derivation scheme is in the following. First, by turning off the coupling (w) between the normal site and the ends of the superconducting nanowire, we find the wavefunctions of the MZMs on the nanowire ends in the presence of the magnetic flux. Then we turn on the weak coupling between

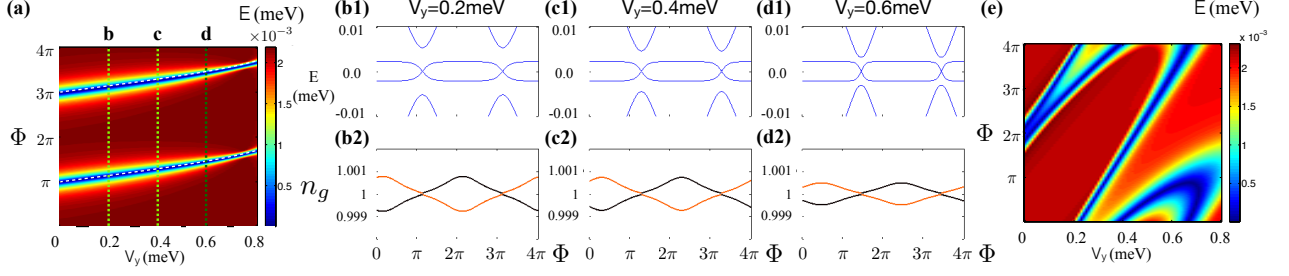


FIG. 6. The physics of the topological superconducting interferometer (a-d) with non-zero Zeeman field (V_y) along the spin orbital coupling is compared with the normal metal interferometer. Panel (a) shows in the topological region at fixed $V_z = 1.2\text{meV}$ the energy level closest to zero energy. The white dashed lines, which are the analytic solution of MZM Φ -location described by eq.17, are consistent with the blue color indicating the MZMs. Panels (1) represent the low energy spectra at the different values of V_y 's. As V_y increases, the MZMs move away from $\Phi = 0, 3\pi$. The conductance peak spacings in panels (2) show that the line crossings reflect the presence of the MZMs. On the other hand, the energy level closest to zero energy in the trivial metal interferometer at $V_z = 1.225\text{meV}$ in panel (e) shows that the zero energy modes (blue color) move differently as V_y varies. The Φ -location of the crossing of the conductance peak spacings is an important observable to distinguish the topological superconductivity and the trivial metal.

the two nanowire ends as a first order perturbation. This perturbation energy can faithfully describe the lowest energy in the topological superconducting interferometer.

We start with the BdG Hamiltonian of the superconducting semiconductor nanowire by Fourier transforming the superconducting part of the Hamiltonian (1) to momentum space

$$H_{\text{BdG}}(k) = [2t(1 - \cos k) - \mu]\tau_z\sigma_0 + \Delta_0\tau_y\sigma_y + V_z\tau_z\sigma_z + V_y\tau_0\sigma_y + 2\alpha\sin k\tau_z\sigma_y \quad (9)$$

We are interested in the low energy theory near the Fermi level as $\mu \approx 2t(1 - \cos k)$. The BdG Hamiltonian can be further simplified to the continuous model

$$H_{\text{BdG}}(k) \approx 2\alpha k\tau_z\sigma_y + \Delta_0\tau_y\sigma_y + V_z\tau_z\sigma_z + V_y\tau_0\sigma_y \quad (10)$$

Since the focus is the low energy mode near one nanowire end ($x = L$), the additional phase Φ of the superconducting order parameter stemming from the magnetic flux can be assumed to be a constant. With this additional phase, the order parameter is given by $\Delta_0 \rightarrow \Delta_0 e^{i\Phi}$. The low energy Hamiltonian can be written as

$$H_{\text{BdG}}(x) = 2\alpha\tau_z\sigma_y \frac{\partial}{i\partial x} + \Delta_0 \cos \Phi \tau_y \sigma_y + \Delta_0 \sin \Phi \tau_x \sigma_y + V_z\tau_z\sigma_z + V_y\tau_0\sigma_y. \quad (11)$$

The two wire ends are located at $x = 0, L$ as domain walls by assuming $\sqrt{\Delta_0^2 - V_y^2} - V_z > 0$ as $0 < x < L$ and $\sqrt{\Delta_0^2 - V_y^2} - V_z < 0$ elsewhere. By solving the eigenvalue problem at zero energy, this assumption leads to an unnormalized MZM wavefunction localized at $x = 0$ without the additional superconducting phase ($\Phi = 0$)

$$|\phi_0\rangle = e^{-\frac{R-V_z}{2\alpha}x} \begin{pmatrix} -ie^{i\beta/2} \\ -ie^{i\beta/2} \\ ie^{-i\beta/2} \\ ie^{-i\beta/2} \end{pmatrix}, \quad (12)$$

where $R = \sqrt{\Delta_0^2 - V_y^2}$ and $\beta = \arctan \frac{V_y}{R}$. In addition, another MZM wavefunction localized at $x = L$ is given by

$$|\phi_L\rangle = e^{\frac{R-V_z}{2\alpha}(x-L)} \begin{pmatrix} ie^{-i\beta/2+i\Phi/2} \\ -ie^{-i\beta/2+i\Phi/2} \\ ie^{i\beta/2-i\Phi/2} \\ -ie^{i\beta/2-i\Phi/2} \end{pmatrix} \quad (13)$$

Since the coupling between the two wire ends is off, as long as the wire length L is long enough, the energies of the two MZMs are close to zero. We turn on the weak coupling between the two ends as the extension of spin orbital coupling

$$\Delta\hat{h} = i\delta(C_0^\dagger\tau_z\sigma_y C_L - C_L^\dagger\tau_z\sigma_y C_0) \quad (14)$$

Consider this term as the first order perturbation, the low energy effective Hamiltonian can be written as the coupling sandwiched by the two MZMs

$$\Delta H = \begin{pmatrix} \langle\phi_0|\Delta\hat{h}|\phi_0\rangle & \langle\phi_0|\Delta\hat{h}|\phi_L\rangle \\ \langle\phi_L|\Delta\hat{h}|\phi_0\rangle & \langle\phi_L|\Delta\hat{h}|\phi_L\rangle \end{pmatrix} \quad (15)$$

$$\propto \delta \sin(\beta - \Phi/2) \begin{pmatrix} 0 & -i \\ i & 0 \end{pmatrix} \quad (16)$$

The energy level crossing (zero energy) occurs as $\Delta H = 0$ at

$$\Phi = (3)\pi + 2\beta. \quad (17)$$

Hence, as $V_y = 0$, the MZMs appear at $\Phi = \pi, 3\pi$; otherwise, the MZMs are not fixed at $\Phi = \pi, 3\pi$.

Back to the simulation of the superconducting ring, we recover the Zeeman field (V_y) along the spin orbital coupling direction and adjust V_z to the topological region. The interferometer ring is still described by the Hamiltonian (1) with non-zero V_z . The energy spectra in Fig. 6(a,1) show that the MZMs move away from

$\Phi = \pi, 3\pi$ and the locations of the MZMs are consistent with the analytic solution (17). Hence, this analytic solution also predicts to the crossing locations of the conductance peak spacings as shown in Fig. 6(2). That is, once the physical values of V_y and Δ_0 , which determine β , are known, if $\Phi = (3)\pi + 2\beta$ are identical to the location of the crossings observed, this directly supports the existence of the MZMs. We can further compare the MZM locations with the lowest energy spectrum of the trivial metal ring as shown in Fig. 6(e). The zero energy modes, which are not the MZMs, lead to the crossings of the conductance peak spacings and the distribution of these zero modes is completely different from the topological superconductor hosting MZMs. Therefore, the locations of the observed crossings can clearly distinguish the topological superconducting interferometer from the trivial metal interferometer.

V. CONCLUSION

As the Zeeman field V_z increases, observing the transition of the phase-current relation from 2π periodicity to

4π periodicity is the preliminary step. However, the transition from a superconductor to a normal metal shares the same periodicity. The details of the observable conductance can exclude the trivial metal scenario. The conductance distribution patterns in the topological region do not alter as a function of V_z , whereas the conductance patterns of the normal metal always change as a function of V_z . In the topological region the line crossing of the conductance peak spacings, which reflect the Φ -location of the MZM, always occurs at $\Phi = \pi, 3\pi$ in the absence of the Zeeman field along the spin orbital coupling direction, while the crossing locations of the trivial metal change with V_z . Even in the presence of the Zeeman field along the spin orbital coupling direction, the Φ -location of the line crossing can be analytically predicted. These conductance interference features can serve to distinguish the topological nanowire ring from a normal metal experimentally.

This work is supported by Microsoft and Laboratory for Physical Sciences.

-
- ¹ J. D. Sau, R. M. Lutchyn, S. Tewari, and S. Das Sarma, Phys. Rev. Lett. **104**, 040502 (2010).
 - ² R. M. Lutchyn, J. D. Sau, and S. Das Sarma, Phys. Rev. Lett. **105**, 077001 (2010).
 - ³ Y. Oreg, G. Refael, and F. von Oppen, Phys. Rev. Lett. **105**, 177002 (2010).
 - ⁴ L. Fu and C. L. Kane, Phys. Rev. Lett. **100**, 096407 (2008).
 - ⁵ V. Mourik, K. Zuo, S. M. Frolov, S. R. Plissard, E. P. A. M. Bakkers, and L. P. Kouwenhoven, Science **336**, 1003 (2012).
 - ⁶ L. P. Rokhinson, X. Liu, and J. K. Furdyna, Nat. Phys. **8**, 795 (2012).
 - ⁷ M. T. Deng, C. L. Yu, G. Y. Huang, M. Larsson, P. Caroff, and H. Q. Xu, Nano Letters **12**, 6414 (2012).
 - ⁸ H. O. H. Churchill, V. Fatemi, K. Grove-Rasmussen, M. T. Deng, P. Caroff, H. Q. Xu, and C. M. Marcus, Phys. Rev. B **87**, 241401 (2013).
 - ⁹ A. Das, Y. Ronen, Y. Most, Y. Oreg, M. Heiblum, and H. Shtrikman, Nat. Phys. **8**, 887 (2012).
 - ¹⁰ A. D. K. Finck, D. J. Van Harlingen, P. K. Mohseni, K. Jung, and X. Li, Phys. Rev. Lett. **110**, 126406 (2013).
 - ¹¹ S. M. Albrecht, A. P. Higginbotham, M. Madsen, F. Kuemmeth, T. S. Jespersen, J. Nygård, P. Krogstrup, and C. M. Marcus, Nature **531**, 206 (2016).
 - ¹² S. D. Sarma, M. Freedman, and C. Nayak, Npj Quantum Information **1**, 15001 EP (2015).
 - ¹³ C. Nayak, S. H. Simon, A. Stern, M. Freedman, and S. Das Sarma, Rev. Mod. Phys. **80**, 1083 (2008).
 - ¹⁴ T. Karzig, C. Knapp, R. M. Lutchyn, P. Bonderson, M. B. Hastings, C. Nayak, J. Alicea, K. Flensberg, S. Plugge, Y. Oreg, C. M. Marcus, and M. H. Freedman, Phys. Rev. B **95**, 235305 (2017).
 - ¹⁵ A. Zazunov, A. L. Yeyati, and R. Egger, Phys. Rev. B **84**, 165440 (2011).
 - ¹⁶ J. D. Sau, B. Swingle, and S. Tewari, Phys. Rev. B **92**, 020511 (2015).
 - ¹⁷ L. Fu, Phys. Rev. Lett. **104**, 056402 (2010).
 - ¹⁸ B. van Heck, R. M. Lutchyn, and L. I. Glazman, Phys. Rev. B **93**, 235431 (2016).
 - ¹⁹ C.-K. Chiu, J. D. Sau, and S. Das Sarma, Phys. Rev. B **96**, 054504 (2017).
 - ²⁰ G. W. Semenoff and P. Sodano, cond-mat/0601261.
 - ²¹ F. K. de Vries, T. Timmerman, V. P. Ostroukh, J. van Veen, A. J. A. Beukman, F. Qu, M. Wimmer, B.-M. Nguyen, A. A. Kiselev, W. Yi, M. Sokolich, M. J. Manfra, C. M. Marcus, and L. P. Kouwenhoven, arXiv:1709.03727 (2017).
 - ²² Y.-L. Lee and Y.-W. Lee, Phys. Rev. B **93**, 184502 (2016).
 - ²³ C. Benjamin and J. K. Pachos, Phys. Rev. B **81**, 085101 (2010).
 - ²⁴ H.-J. Kwon, K. Sengupta, and V. M. Yakovenko, The European Physical Journal B - Condensed Matter and Complex Systems **37**, 349 (2004).
 - ²⁵ M. Cheng and R. Lutchyn, Phys. Rev. B **92**, 134516 (2015).
 - ²⁶ A. Kitaev, Physics Uspekhi **44**, 131 (2001).
 - ²⁷ S. Rubbert and A. R. Akhmerov, Phys. Rev. B **94**, 115430 (2016).
 - ²⁸ D. V. Averin, Phys. Rev. Lett. **82**, 3685 (1999).
 - ²⁹ J. R. Williams, A. J. Bestwick, P. Gallagher, S. S. Hong, Y. Cui, A. S. Bleich, J. G. Analytis, I. R. Fisher, and D. Goldhaber-Gordon, Phys. Rev. Lett. **109**, 056803 (2012).
 - ³⁰ A. Yamakage, M. Sato, K. Yada, S. Kashiwaya, and Y. Tanaka, Phys. Rev. B **87**, 100510 (2013).
 - ³¹ C. Kurter, A. D. K. Finck, Y. S. Hor, and D. J. Van Harlingen, Nat. Commun. **6**, 7130 (2015).
 - ³² L. Fu and C. L. Kane, Phys. Rev. B **79**, 161408 (2009).